Super-long span bridge aerodynamics benchmark: additional results for TG3.1 Step 1.2

Giorgio DIANA
Chair of Task Group 3.1
Politecnico di Milano, Italy

Stoyan STOYANOFF
Vice-chair of Task Group 3.1
RWDI, Canada

Andrew ALLSOP
ARUP
United-Kingdom

Luca AMERIO
ARUP
United-Kingdom

Tommaso ARGENTINI
Politecnico di Milano
Italy

Miguel CID MONTOYA
University of A Coruna
Spain

Vincent De Ville
GREISCH
Belgium

Michael Stirk Andersen
Svend Ole Hansen ApS
Denmark

Santiago HERNÁNDEZ
University of A Coruna
Spain

José Ángel JURADO
University of A Coruna
Spain

Igor KAVRAKOV
Bauhaus-University Weimar
Germany

Guy LAROSE
RWDI
Canada

Allan LARSEN
COWI
Denmark

Guido MORGENTHAL
Bauhaus-University Weimar
Germany

Simone OMARINI
Politecnico di Milano
Italy

Daniele ROCCHI
Politecnico di Milano
Italy

Martin SVENDSEN
Ramboll
Denmark

Contact: daniele.rocchi@polimi.it

Abstract

This paper presents the ongoing benchmark results of IABSE Task Group 3.1. The task of this working group is to create benchmark results for the validation of methodologies and software programs developed to assess the stability and the buffeting response of long span bridges. Indeed, accurate estimations of structural stability and response to strong winds are critical for the successful design of long-span bridges. While the first results of the benchmark, dealing with a section approach, have been already published, in this paper the ongoing activity and results of the task group are presented. The topic of these results is the numerical response of a full-bridge model under the actions of a multi-correlated wind field both in terms of aeroelastic stability and buffeting response.

Keywords: benchmark; aeroelasticity; flutter; buffeting; long-span bridge.

1 Introduction

IABSE Task Group 3.1 (TG) goal is the definition of a procedure for validating the software programs for computing the bridge response to turbulent wind. The procedure is composed of steps with an increasing level of complexity fully described in [1] and [2] together with the first set of results.

The idea is to compare the results, TG partners obtain using different numerical models, simulating different case studies by using the same set of input data. The results are then used as a base to produce reference data for software validation.

In this paper, the aeroelastic response of a full bridge model to a multi-correlated wind field (Step 1.2) is considered, and a comparison among the already collected results is presented.

The task is not completed and the collection of the contribution from the TG partners is still on going but the presented results in addition to those shown in [6] represent the evolution of TG work.

2 Benchmark: Step 1.2

2.1 Step 1.2 Cases

Step 1.2 is divided in two sub-cases with increasing complexity. Both cases study the stability and the buffeting response of the Storebælt bridge, forced by a turbulent wind field, where the horizontal and vertical components of wind velocity change in time and space (along the bridge axis). Aerodynamic forces are considered only on the deck.

a) Step 1.2a does not consider the static deflection of the bridge and experimental aerodynamic coefficients are taken at 0-degree angle of attack for all the deck section.
b) Step 1.2b considers the static deflection of the bridge and the dependency of the experimental aerodynamic coefficients upon the angle of attack.

In this paper, selected preliminary results of Step 1.1a-b are presented.

2.2 Input for the analysis Step 1.2

2.2.1 Structural data

The bridge is modelled through a modal approach considering the first 12 modes of vibrationwhose natural frequencies are reported in Table 1. The mode shapes are also shared among TG participants.

Table 1. Modal parameters

#	Mode	Frequency [Hz]	Damping ξ [-]
1	horizontal 1	0.0521	0.3%
2	vertical 1	0.0839	0.3%
3	vertical 2	0.0998	0.3%
4	horizontal 2	0.1179	0.3%
5	vertical 3	0.1317	0.3%
6	vertical 4	0.1345	0.3%
7	vertical 5	0.1827	0.3%
8	horizontal 3	0.1866	0.3%
9	torsional 1	0.2784	0.3%
10	vertical 6	0.2815	0.3%
11	torsional 2	0.3833	0.3%
12	vertical 7	0.3975	0.3%

2.2.2 Incoming turbulent wind

Wind input is also an input shared among TG participants. Spectra and statistical parameters are reported in Table 2 and the space coherence between *u* or *w* at two different points *P* and *Q* is:

$$\Lambda_{ii} = \exp\left(-\frac{2\sqrt{(C_{iz}\Delta_x)^2+(C_{iz}\Delta z)^2}\,f}{\overline{U_P}+\overline{U_Q}}\right) \quad (1)$$

where $i = u$ or w, $C_{ux} = 10$, $C_{uz} = 10$, $C_{wx} = 6.50$, $C_{wz} = 3$, $\Delta z = z_P - z_Q$ and $\Delta x = x_P - x_Q$.

More over, ten time histories of turbulent wind velocities were generated ([7]) in the 90 wind sections reported with red lines in Figure 1, using the same wind characteristics, to allow the use of time-domain approaches. Each time history is 10 minute long with a sampling frequency of 20 Hz. For the 45 m/s case, longer time histories 1-hour long are also provided to account for low frequency contributions.

Table 2. Incoming wind characteristics

Wind speeds	U = 15, 30, 45, 60, 75 m/s
Air density	$\rho = 1.22$ kg/m^3
Turbulence intensity	$I_u = \frac{\sigma_u}{U} = 0.10$; $I_w = \frac{\sigma_w}{U} = 0.05$
Integral length scale	^xL_u = 200 m; ^xL_w = 20 m
***u* and *w* spectra**	$\frac{f \cdot S_u(f)}{\sigma_u^2} = \frac{4\left(\frac{f\,{}^xL_u}{U}\right)}{\left[1+70.8\left(\frac{f\,{}^xL_u}{U}\right)^2\right]^{5/6}}$ $\frac{f \cdot S_w(f)}{\sigma_w^2} = \frac{4\left(\frac{f\,{}^xL_w}{U}\right)\left(1+755.2\left(\frac{f\,{}^xL_w}{U}\right)^2\right)}{\left[1+283.2\left(\frac{f\,{}^xL_w}{U}\right)^2\right]^{11/6}}$ $S_{uw}(f) = 0$

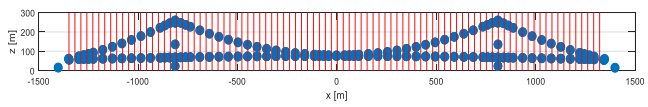

Figure 1. Full bridge and wind sections (red lines)

2.2.3 Aerodynamic forces

For sake of simplicity, aerodynamic forces are considered only on the deck. Sign conventions for forces and displacements are shown in Figure 2.

For sake of completeness, the set of experimental aerodynamic coefficients of the Yavuz Sultan Selim Bridge (Third Bosphorus Bridge) without windscreens are considered [5].

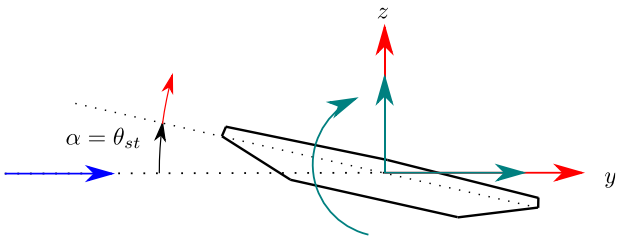

a) deck forces and displacements

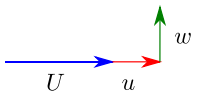

b) turbulent wind

Figure 2. Sign conventions

The steady aerodynamic drag, lift and moment coefficient per unit length as functions of the angle of attack α are defined as:

$$F_{ST} = \frac{1}{2}\rho U^2 B \begin{bmatrix} C_D(\alpha) \\ C_L(\alpha) \\ B\,C_M(\alpha) \end{bmatrix} \quad (2)$$

where $B = 31m$ is the deck chord, U the mean wind velocity, and ρ the air density. C_D, C_L, C_M are respectively the drag, lift and moment static coefficients, reported in Figure 3.

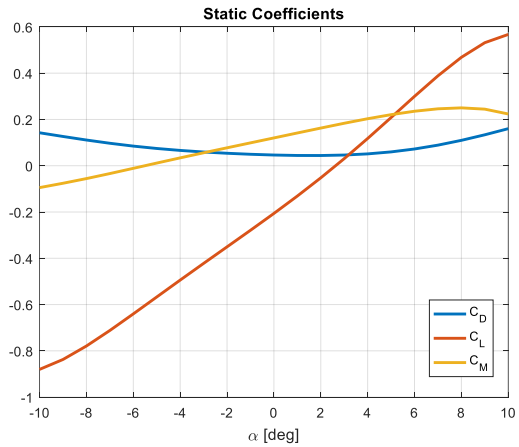

Figure 3. Static coefficients

The aeroelastic forces (self-excited forces F_{se}) per unit length are defined through the flutter derivatives reported below in the Polimi formulation:

$$D_{se} = \frac{1}{2}\rho U^2 B \begin{pmatrix} -p_1^* \frac{\dot{z}}{U} - p_2^* \frac{B\dot{\theta}}{U} + p_3^* \theta + \dots \\ \frac{2\pi^3}{V^{*2}} p_4^* \frac{z}{B} - p_5^* \frac{\dot{y}}{U} + \frac{2\pi^3}{V^{*2}} p_6^* \frac{y}{B} \end{pmatrix} \quad (3)$$

$$L_{se} = \frac{1}{2}\rho U^2 B \begin{pmatrix} -h_1^* \frac{\dot{z}}{U} - h_2^* \frac{B\dot{\theta}}{U} + h_3^* \theta + \dots \\ \frac{2\pi^3}{V^{*2}} h_4^* \frac{z}{B} - h_5^* \frac{\dot{y}}{U} + \frac{2\pi^3}{V^{*2}} h_6^* \frac{y}{B} \end{pmatrix} \quad (4)$$

$$M_{se} = \frac{1}{2}\rho U^2 B^2 \begin{pmatrix} -a_1^* \frac{\dot{z}}{U} - a_2^* \frac{B\dot{\theta}}{U} + a_3^* \theta + \dots \\ \frac{2\pi^3}{V^{*2}} a_4^* \frac{z}{B} - a_5^* \frac{\dot{y}}{U} + \frac{2\pi^3}{V^{*2}} a_6^* \frac{y}{B} \end{pmatrix} \quad (5)$$

The eight flutter derivatives coefficients $(a_1^*, a_2^*, a_3^*, a_4^*, h_1^*, h_2^*, h_3^*, h_4^*)$ are provided at five mean angles of attack: -4 deg, -2 deg, 0 deg, +2 deg, +4 deg, in the reduced velocity range $1<V^* = U/(fB) < 17$, being f the motion frequency.

The flutter derivatives p_{1-6}^*, a_{5-6}^*, h_{5-6}^* are derived from quasi steady theory (QST) to complete the full set of aerodynamic coefficients.

The buffeting forces F_{buff} per unit length due to incoming turbulent wind components u and w are defined in frequency domain through admittance functions:

$$\begin{Bmatrix} D_{buff} \\ L_{buff} \\ M_{buff} \end{Bmatrix} = \frac{1}{2}\rho U B \begin{bmatrix} \chi^*_{Du} & \chi^*_{Dw} \\ \chi^*_{Lu} & \chi^*_{Lw} \\ B\chi^*_{Mu} & B\chi^*_{Mw} \end{bmatrix} \begin{Bmatrix} U_u(f) \\ W_w(f) \end{Bmatrix} \quad (6)$$

Where $U_u(f)$ is the Fourier transform of $u(t)$ and $W_w(f)$ the Fourier transform of $w(t)$; χ^* are the admittance functions. The χ^* are defined using the quasi-steady values weighed by the Davenport function $A(V*)$ as:

$$\begin{aligned} \chi^*_{Du} &= 2C_D\, A(f^*) \\ \chi^*_{Lu} &= 2C_L\, A(f^*) \\ \chi^*_{Mu} &= 2C_M\, A(f^*) \\ \chi^*_{Dw} &= (K_D - C_L) A(f^*) \\ \chi^*_{Lw} &= (K_L + C_D) A(f^*) \\ \chi^*_{Mw} &= K_M\, A(f^*) \end{aligned} \quad (7)$$

where $A(V^*)$ is a real weighing function in reduced velocity:

$$A(V^*) = \frac{2}{(7/V^*)^2}\left(7/V^* - 1 + e^{-7/V^*}\right) \quad (8)$$

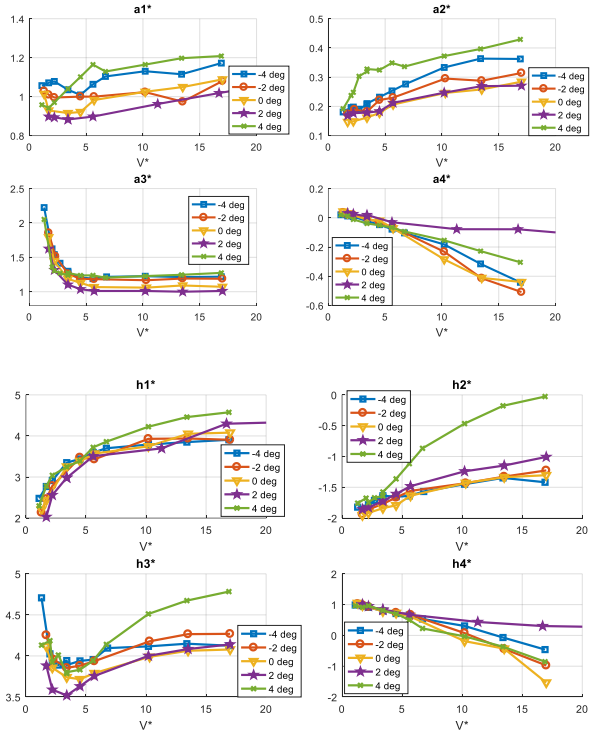

Figure 4. Flutter derivative coefficients

2.3 Required output for Step1.2 a/b

To perform the benchmark among the results and produce reference data for numerical codes validation, the following results are considered for both Cases a) and b):

1 Flutter stability:
   a. Critical flutter speed;
   b. frequencies and damping as a function of mean wind speed.
2 Buffeting response to turbulent wind:
   a. standard deviation of the displacement at mid span and at quarter span as a function of mean wind speed;
   b. Comparison of power spectral densities (PSD) of the displacement at mid span and at quarter span as function of mean wind speed.

3 Results of Step 1.2a

Only a small selection of results is presented in this paper, while the full set of results will be presented in a future work in the IABSE SEI journal as already done for the previous Steps ([1], [2]).

Each contribution is defined anonymously by a number.

3.1 Step1.2a – Flutter speed

Figure 5 shows 12 contributions for the assessment of the flutter speed of the considered bridge.

As an attempt to define a reference value for numerical code validation and an associated band of acceptance, on the basis of the collected results, the following procedure is applied:

1. The mean μ^* (red dash dot line) and the standard deviation σ^* of all data is computed.
2. The data outside $\mu^* \pm \sigma^*$ (red dash lines) are considered outlier data.
3. The reference mean value μ (dash black line) and standard deviation σ are computed excluding the outlier data.

As criterion of numerical code validation, results within $\mu \pm \sigma$ (black dot lines) are considered valid. Considering the available contributions, the reference values are: μ = 69.8 m/s and σ = 0.6 m/s.

These values will be refined once all the participants will provide their results. For six of the contributions, Figure 6 also shows the trend of frequency and damping for the mode that shows flutter instability: even though the spread of the flutter speed parameter is small larger differences can be noted in the trend of the damping ratio vs mean wind speed denoting a different modelling of this aeroelastic effect.

3.2 Step1.2a – RMS displacements

Figure 7 shows seven different contributions for the trend on RMS values of the vertical displacement and torsional displacement at mid span increasing the mean wind speed. Results coming from both time domain (TD) and frequency domain (FD) methods are present.

Torsional displacement is expressed as the displacement of the windward edge of the deck $z_{eq} = \frac{B}{2}\theta$. It is possible to notice that results are quite consistent, especially up to 45 m/s

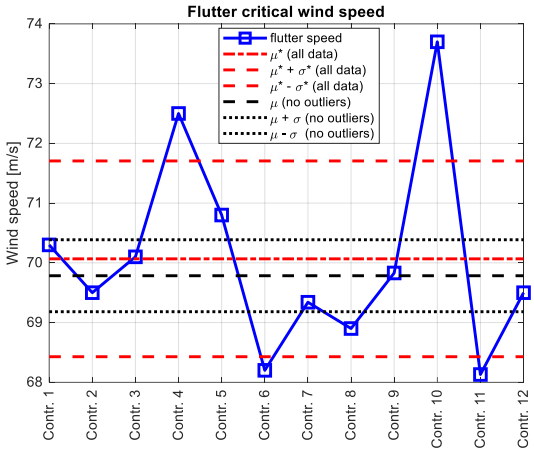

Figure 5. Step 1.2a Flutter critical wind speed results

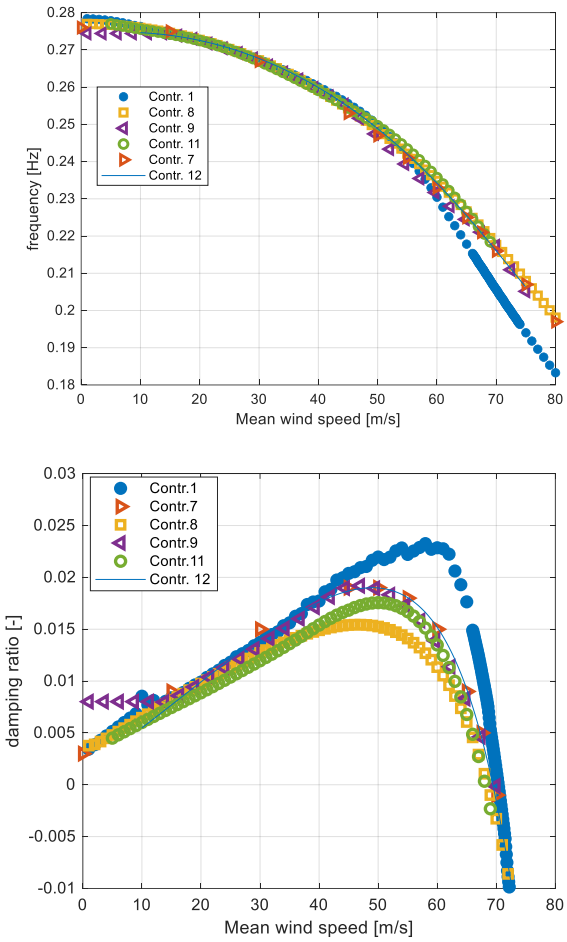

Figure 6. Step 1.2a Trend of frequency and damping for the mode that shows flutter instability.

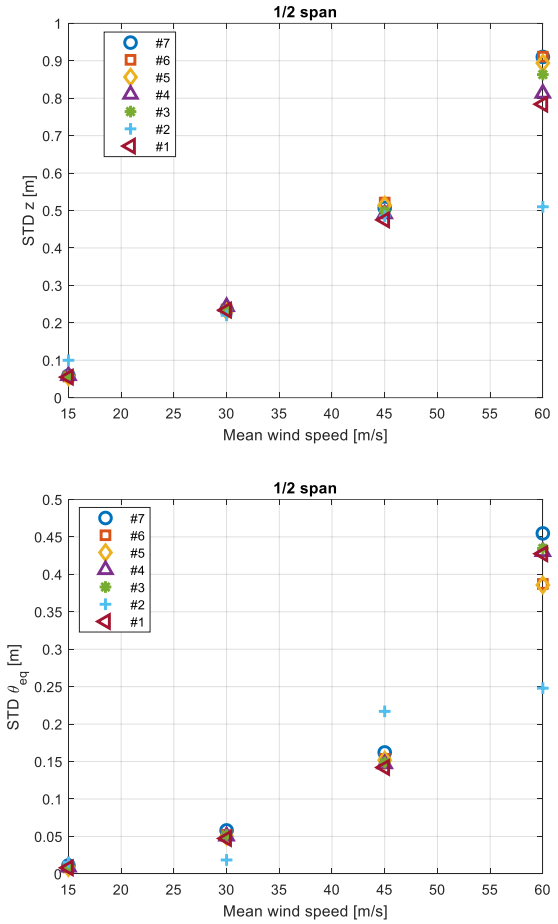

Figure 7. Step 1.2a RMS of the vertical and torsional displacement at midspan vs. wind speed

3.3 Step1.2a – PSD of physical displacements at midspan

Another way to compare results is proposed in Figure 8 where the PSDs of the vertical and torsional displacement of the midspan deck section at 45 m/s are reported. Looking at the rotations it seems that the major difference is in the estimate of the resonant response. Looking at the vertical motion, contributions #3 and #4 have smaller values in the low frequency part, and this would not have been noticed looking only at the std values that are similar to the others.

4 Results of Step 1.2b

Some results for Step 1.2b are shown in the following, compared to the corresponding for Step 1.2a: static rotation of deck, flutter speed, time histories of midspan vertical displacements for 30 and 45 m/s.

Figure 9 shows six different results for the deck static rotation as a function of the wind speed: two contributions have scatter results and further investigations are therefore going on.

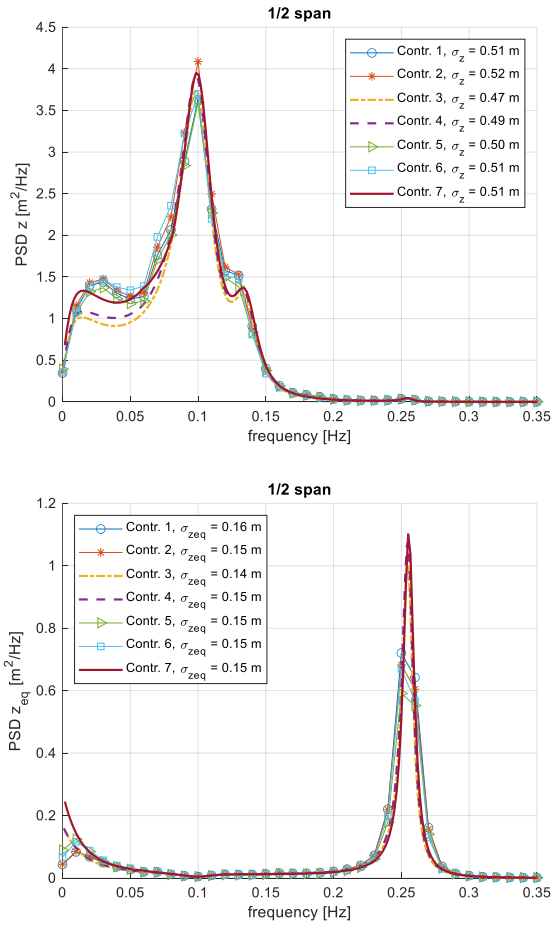

Figure 8. PSD the vertical and torsional displacement at midspan at 45 m/s

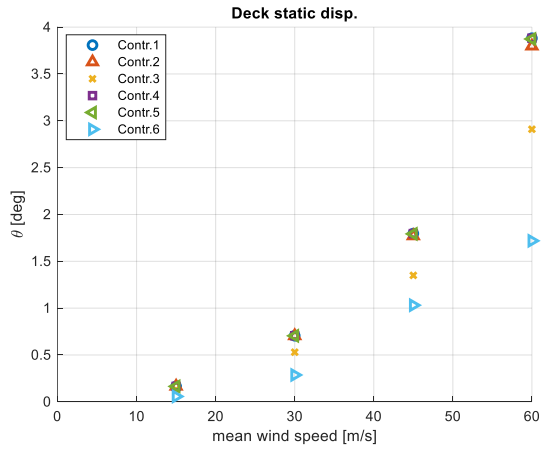

Figure 9. Step 1.2b midspan static rotation as a function of wind speed

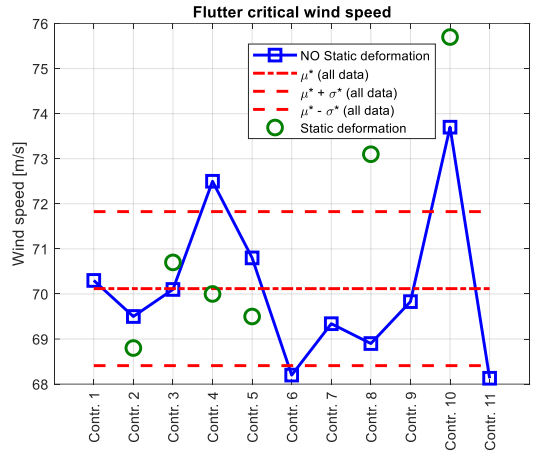

Figure 10. Step 1.2b Flutter critical wind speed results, compared to Step 1.2a

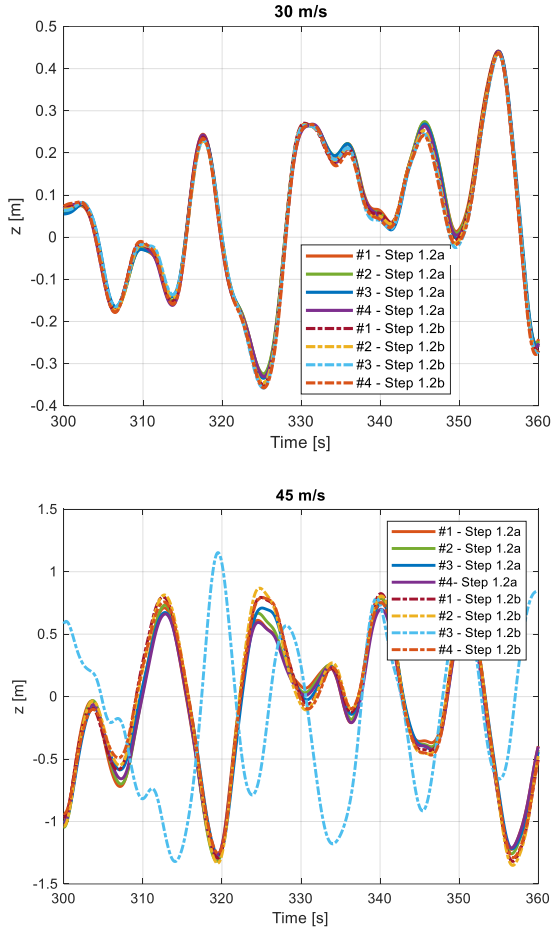

Figure 11. Step 1.2b Example of time histories for midspan vertical displacement and rotation at 30 m/s

Figure 10 shows the effect of considering the mean static rotation on flutter speed: the results seem more scattered and not all in the same direction. More contributions are needed to better assess the results.

Figure 11 compares the performances of different time domain methods, for two different mean wind speeds. At 30 m/s it seems that results for 1.2a and 1.2b are overlapped: the is because the static rotation of the deck is less than 1 deg with negligible effect on the value of the aeroelastic coefficients. At 45 m/s, where the midspan static rotation is 2 deg, on the contrary, one model behaves differently from the others. Also in this case a deeper investigation is required to better understand.

5 Conclusions

This paper presents ongoing results of Step 1.2 of the benchmark study: even for this rather simple problem, noticeable differences arose during the result comparisons.

For 1.2a, similar critical flutter velocities and RMS were predicted. Removing the outliners, most of the remaining predictions are reasonably close and the results within the interval $\mu \pm \sigma$ appear reasonable.

For case 1.2b more contributions are needed to draw conclusions, but it seems that the change in the mean angle of attack has little influence, considering the input parameters selected for this benchmark.

6 References

[1] Diana, G.; Stoyanoff, S.; Aas-Jakobsen, K.; Allsop, A.; Andersen, M.; Argentini, T.; Montoya, M. C.; Hernández, S.; Jurado, J. Á.; Katsuchi, H.; Kavrakov, I.; Kim, H.-K.; Larose, G.; Larsen, A.; Morgenthal, G.; Øiseth, O.; Omarini, S.; Rocchi, D.; Svendsen, M. & Wu, T. IABSE Task Group 3.1 Benchmark Results. Part 1: Numerical Analysis of a Two-Degree-of-Freedom Bridge Deck Section Based on Analytical Aerodynamics. Structural Engineering International, Taylor & Francis, 2019, 30, 401-410

[2] Diana, G.; Stoyanoff, S.; Aas-Jakobsen, K.; Allsop, A.; Andersen, M.; Argentini, T.;

Montoya, M. C.; Hernández, S.; Jurado, J. Á.; Katsuchi, H.; Kavrakov, I.; Kim, H.-K.; Larose, G.; Larsen, A.; Morgenthal, G.; Øiseth, O.; Omarini, S.; Rocchi, D.; Svendsen, M. & Wu, T. IABSE Task Group 3.1 Benchmark Results. Part 2: Numerical Analysis of a Three-Degree-of-Freedom Bridge Deck Section Based on Experimental Aerodynamics Structural Engineering International, Taylor & Francis, 2019, 30, 411-420

[3] Diana G, Rocchi D, and Argentini T. Buffeting response of long span bridges: numerical-experimental validation of fluid-structure interaction models *IABSE Conference - Structural Engineering: Providing Solutions to Global Challenges,* 2015

[4] Aas-Jakobsen, K.; Allsop, A.; Kavrakov, I.; Larsen, A.; Øiseth, O.; Argentini, T.; Diana, G.; Omarini, S.; Rocchi, D.; Svendsen, M.; Larose, G.; Stoyanoff, S.; Kim, H.-K.; Hernandez; Wu, T.; Andersen, M. & Katsuchi, H. Super-long span bridge aerodynamics: First results of the numerical benchmark tests from task group 10 *IABSE Symposium, Nantes 2018: Tomorrow's Megastructures*, 2019, S34-71-S34-82

[5] Diana, G.; Rocchi, D.; Argentini, T. & Omarini, S. Flutter derivatives identification on a very large scale aeroelastic deck model *IABSE Conference, Vancouver 2017: Engineering the Future - Report*, 2017, 1997-2005

[6] Diana, G.; Stoyanoff, S.; Allsop, A.; Amerio, L.; Argentini, T.; Cid Montoya, M.; Hernández, S.; Jurado, J. Á.; Kavrakov, I.; Larose, G.; Larsen, A.; Morgenthal, G.; Omarini, S.; Rocchi, D. & Svendsen, M. *Super-long span bridge aerodynamics: on-going results of the TG3.1 benchmark test -- Step 1.2*, 20th Congress of IABSE, New York City 2019: The Evolving Metropolis - Report, 2019, 2645-2650

[7] Deodatis G. Simulation of ergodic multivariate stochastic processes. *Journal of Engineering Mechanics*. 1996; **122:**778-787.